doi:10.1093/brain/awaa019 BRAIN 2020: 143; 944–959 | 944

BRAIN
A JOURNAL OF NEUROLOGY

Network degeneration in Parkinson's disease: multimodal imaging of nigro-striato-cortical dysfunction

Marina C. Ruppert,[1,2,*] Andrea Greuel,[1,*] Masoud Tahmasian,[3] Frank Schwartz,[4] Sophie Stürmer,[5,6] Franziska Maier,[7] Jochen Hammes,[8] Marc Tittgemeyer,[5,9] Lars Timmermann,[1,2] Thilo van Eimeren,[6,8,10,11] Alexander Drzezga[8,11,12] and Carsten Eggers[1,2]

[*]These authors contributed equally to this work.

The spreading hypothesis of neurodegeneration assumes an expansion of neural pathologies along existing neural pathways. Multimodal neuroimaging studies have demonstrated distinct topographic patterns of cerebral pathologies in neurodegeneration. For Parkinson's disease the hypothesis so far rests largely on histopathological evidence of α-synuclein spreading in a characteristic pattern and progressive nigrostriatal dopamine depletion. Functional consequences of nigrostriatal dysfunction on cortical activity remain to be elucidated. Our goal was to investigate multimodal imaging correlates of degenerative processes in Parkinson's disease by assessing dopamine depletion and its potential effect on striatocortical connectivity networks and cortical metabolism in relation to parkinsonian symptoms. We combined ^{18}F-DOPA-PET, ^{18}F-fluorodeoxyglucose (FDG)-PET and resting state functional MRI to multimodally characterize network alterations in Parkinson's disease. Forty-two patients with mild-to-moderate stage Parkinson's disease and 14 age-matched healthy control subjects underwent a multimodal imaging protocol and comprehensive clinical examination. A voxel-wise group comparison of ^{18}F-DOPA uptake identified the exact location and extent of putaminal dopamine depletion in patients. Resulting clusters were defined as seeds for a seed-to-voxel functional connectivity analysis. ^{18}F-FDG metabolism was compared between groups at a whole-brain level and uptake values were extracted from regions with reduced putaminal connectivity. To unravel associations between dopaminergic activity, striatocortical connectivity, glucose metabolism and symptom severity, correlations between normalized uptake values, seed-to-cluster β-values and clinical parameters were tested while controlling for age and dopaminergic medication. Aside from cortical hypometabolism, ^{18}F-FDG-PET data for the first time revealed a hypometabolic midbrain cluster in patients with Parkinson's disease that comprised caudal parts of the bilateral substantia nigra pars compacta. Putaminal dopamine synthesis capacity was significantly reduced in the bilateral posterior putamen and correlated with ipsilateral nigral ^{18}F-FDG uptake. Resting state functional MRI data indicated significantly reduced functional connectivity between the dopamine depleted putaminal seed and cortical areas primarily belonging to the sensorimotor network in patients with Parkinson's disease. In the inferior parietal cortex, hypoconnectivity in patients was significantly correlated with lower metabolism (left $P = 0.021$, right $P = 0.018$). Of note, unilateral network alterations quantified with different modalities corresponded with contralateral motor impairments. In conclusion, our results support the hypothesis that degeneration of nigrostriatal fibres functionally impairs distinct striatocortical connections, disturbing the efficient interplay between motor processing areas and impairing motor control in patients with Parkinson's disease. The present study is the first to reveal trimodal evidence for network-dependent degeneration in Parkinson's disease by outlining the impact of functional nigrostriatal pathway impairment on striatocortical functional connectivity networks and cortical metabolism.

Received August 28, 2019. Revised November 21, 2019. Accepted December 11, 2019. Advance Access publication February 14, 2020

1 Department of Neurology, University Hospital of Marburg, Germany
2 Center for Mind, Brain and Behavior - CMBB, Universities Marburg and Gießen, Germany
3 Institue of Medical Science and Technology, Shahid Beheshti University, Tehran, Iran
4 Department of Neurology, Hospital of the Brothers of Mercy, Trier, Germany
5 Max Planck Institute for Metabolism Research, Cologne, Germany
6 Department of Neurology, Medical Faculty and University Hospital Cologne, University Hospital Cologne, Germany
7 Department of Psychiatry, University Hospital Cologne, Medical Faculty, Cologne, Germany
8 Multimodal Neuroimaging Group, Department of Nuclear Medicine, Medical Faculty and University Hospital Cologne, University Hospital Cologne, Germany
9 Cluster of Excellence in Cellular Stress and Aging Associated Disease (CECAD), Cologne, Germany
10 Cognitive Neuroscience, Institute of Neuroscience and Medicine (INM-3), Research Center Jülich, Germany
11 German Center for Neurodegenerative Diseases (DZNE), Germany
12 Cognitive Neuroscience, Institute of Neuroscience and Medicine (INM-2), Research Center Jülich, Germany

Correspondence to: Univ-Prof. Dr Carsten Eggers
Department of Neurology
University Hospital of Marburg
Baldingerstraße
35033 Marburg
Germany
E-mail: marina.ruppert@uni-marburg.de or Andrea.greuel@med.uni-marburg.de

Keywords: neurodegeneration; network degeneration; Parkinson's disease; multimodal imaging

Abbreviations: BOLD = blood oxygen level-dependent; DMN = default mode network; FDG = fluorodeoxyglucose; IPC = inferior parietal cortex; LEDD = levodopa equivalent daily dose; MMSE = Mini-Mental State Examination; ROI = region of interest; SN(pc) = substantia nigra (pars compacta); UPDRS = Unified Parkinson's Disease Rating Scale

Introduction

Although consequences of selective neural cell death in the substantia nigra pars compacta (SNpc) gave rise to landmark insights into Parkinson's disease pathophysiology by identifying an imbalance between motor-inhibiting and motor-promoting pathways (Kish *et al.*, 1988; Albin *et al.*, 1989; DeLong, 1990), they are not capable of clarifying the entire spectrum of parkinsonian symptoms. Therefore, a more systemic approach is needed as Parkinson's disease is a multifarious disorder, characterized by a complex pattern of progressively worsening symptoms (Obeso *et al.*, 2017). Choosing a unique methodological approach, Braak and colleagues were the first to systematically map stages of Parkinson's disease pathology based on post-mortem examination of cerebral α-synuclein distribution. As the SNpc is not affected until Braak stage 3 and neocortical areas become involved much later, their observations are suggestive of an ascending progressive pathology (Braak *et al.*, 2003).

Based on the assumption that neural pathologies spread out along existing networks, the network degeneration hypothesis of neurodegeneration has moved into the focus of research in the past decade (Palop *et al.*, 2006; Seeley *et al.*, 2009; Tahmasian *et al.*, 2016; Drzezga, 2018; Bischof *et al.*, 2019). Multimodal neuroimaging studies have reported a spatial coincidence between patterns of brain atrophy in several forms of dementia and functional network organization in healthy subjects (Seeley *et al.*, 2009). Accumulating evidence suggests a distinct topographic aggregation of molecular, structural and functional abnormalities in Alzheimer's disease (Bischof *et al.*, 2016; Dronse *et al.*, 2017), preferentially detectable within specific brain networks (Buckner *et al.*, 2005; Zhou *et al.*, 2012; Hoenig *et al.*, 2018). More precisely, disturbances in functional connectivity were found to arise at important densely connected network 'hubs' (Drzezga *et al.*, 2011), which also have been reported to exhibit a higher tau and amyloid burden (Buckner *et al.*, 2009; Cope *et al.*, 2018).

Unfortunately, because of the lack of reliable α-synuclein tracers, functional neuroimaging techniques are not capable of specifically tracing α-synuclein distribution in the living human Parkinson's brain. However, in contrast to histopathological studies, functional neuroimaging allows longitudinal monitoring of cerebral pathologies, which may reflect indirect functional correlates of selective neural cell death and unravel disease mechanisms implicated in aetiology and disease progression (Politis, 2014; Pagano *et al.*, 2016). Using ^{18}F-fluorodeoxyglucose (FDG)-PET, a metabolic spatial covariance pattern, the Parkinson's disease-related pattern, has been repeatedly validated in populations of patients with Parkinson's disease (Schindlbeck and Eidelberg, 2018). It is characterized by increased activity in pallidothalamic, pontocerebellar and primary motor regions, and reduced activity in premotor cortex, supplementary motor and parietal association areas (Niethammer and Eidelberg, 2012).

Dopaminergic deficits in Parkinson's disease can reliably be assessed *in vivo* by ^{18}F-DOPA-PET and typically are most severe in the posterior putamen (Sawle *et al.*, 1994).

Despite their high sensitivity for diagnosis, no first-line diagnostic neuroimaging tool has been established for clinical practice; metabolic and dopaminergic imaging are still considered as adjuvant tools (Politis, 2014).

In Parkinson's disease, denervation of striatal structures—mainly the putamen—and consequential neurochemical alterations in the basal ganglia are hypothesized to impair functional integrity of remote brain regions, which may be involved in motor symptoms (Wu *et al.*, 2009). In accordance with known patterns of neural degeneration within the basal ganglia, dysfunctional resting activity of the posterior putamen is hypothesized to underlie motor abnormalities seen in Parkinson's disease (Hacker *et al.*, 2012). There is also growing interest in dysfunctional connectivity that extends beyond the sensorimotor network, affecting e.g. the default mode network (DMN), as possible correlates of non-motor symptoms, including cognitive impairment (Prodoehl *et al.*, 2014). Functional network alterations in resting state functional MRI in Parkinson's disease have been analysed with different methodological approaches, including seed-based analysis (Helmich *et al.*, 2010; Prodoehl *et al.*, 2014; Tahmasian *et al.*, 2015*a*, 2017; Mohan *et al.*, 2016) or multivariate network approaches (Ghasemi and Mahloojifar, 2013; Cerasa *et al.*, 2016; Vo *et al.*, 2017; Ehgoetz Martens *et al.*, 2018). For instance, a functional connectivity equivalent of the Parkinson's disease-related pattern was recently detected using independent component analysis (Vo *et al.*, 2017), highlighting the capability of resting state functional MRI to unravel pathological correlates of motor dysfunction and non-motor symptoms (Schindlbeck and Eidelberg, 2018).

Cross-modal inspection of cerebral pathologies identified by different imaging methods in the same subjects holds the potential to uncover pathophysiological mechanisms and topographic overlaps of different degenerative processes (Drzezga *et al.*, 2011; Bischof *et al.*, 2016; Hoenig *et al.*, 2018). Associations between different cerebral pathological features identified by functional imaging in Parkinson's disease have not been thoroughly examined so far and therefore are poorly understood. In particular, the extent to which topographically preceding pathologies such as nigral degeneration and putaminal dopamine depletion affect cortical abnormalities and their putative effect on parkinsonian symptoms remains to be elucidated to clarify if network degeneration is at play and pave the way for developing multimodal imaging markers as diagnostic and progression tracking tools.

Materials and methods

Subject inclusion and clinical assessment

After declaring informed consent in conformation with the Declaration of Helsinki and according to the institutional guidelines of the local ethics committee (ethical clearance number EK12-265), 25 healthy controls and 60 patients with idiopathic Parkinson's disease, diagnosed according to the UK Brain Bank criteria, were included. Subjects were recruited via the neurological outpatient clinic at the University Hospital of Cologne and associated neurological practices. Healthy control subjects were reached by advertising. For PET imaging, the Federal Bureau for Radiation gave permission to apply radiation in patients and healthy controls. Exclusion criteria were age <40 years, suspected atypical parkinsonian syndromes, advanced parkinsonism [i.e. Hoehn and Yahr stage >3 (Hoehn and Yahr, 1967)], dementia, CNS diseases other than Parkinson's disease, and any safety concerns for MRI scanning. Dementia was excluded according to criteria published by the Movement Disorder Society by using a neuropsychological test battery and an assessment of the patient's ability to manage daily life (Emre *et al.*, 2007). Global cognitive screening was performed using the Mini-Mental State Examination (MMSE) (Folstein *et al.*, 1975). Functional, anatomical and clinical data were collected at the Max Planck institute for Metabolism Research Cologne and the University Hospital Cologne, Department of Neurology. MRI images were acquired from all subjects, while limited numbers of subjects were available for PET imaging (Table 1). Levodopa-equivalent daily dose (LEDD) was calculated for total antiparkinsonian medication and separately for dopamine agonists based on standard conventions (Tomlinson *et al.*, 2010). Clinical examination and functional imaging were carried out in the OFF state, defined as a 12-h period without dopaminergic medication (Langston *et al.*, 1992) (72 h in cases of dopamine agonists). Disease severity was quantified by the Unified Parkinson's Disease Rating Scale (UPDRS) part III (Fahn *et al.*, 1987). Subscores for akinesia-rigidity were calculated for the whole body and left/right hemibody from subsets of UPDRS-III items (Supplementary material). Subdivision of patients into tremor-dominant and non-tremor-dominant subtypes was performed according to strict criteria as previously described (Eggers *et al.*, 2011) (Supplementary material).

Image acquisition and analysis

^{18}F-FDG- and ^{18}F-DOPA-PET

All PET scans were acquired on an ECAT HRRT-PET-Scanner (CTI) at the Max-Planck-Institute for Metabolism Research in Cologne. Both ^{18}F-FDG- and ^{18}F-DOPA-PET were performed within a 2-day interval, each in the morning after overnight fasting and OFF dopaminergic medication. In case of ^{18}F-DOPA, 100 mg of carbidopa was administered 1 h before tracer injection. Otherwise, except for scan duration, protocols were identical for both PET scans, as follows. Under standardized conditions (dimmed light, closed eyes, quiet room) subjects were positioned along the kantho-meatal line. Following a transmission scan, 185 MBq of the radioligand was injected intravenously and tomographic images were acquired in a dynamic PET scan (60 min for ^{18}F-FDG and 90 min for ^{18}F-DOPA). Using camera-specific filters, PET data were corrected for attenuation and scattered radiation, and reconstructed to 207 slices with a 256×256 matrix and 1.22 mm voxel size, creating one frame per 10 min. Frames were realigned for motion correction by rigid-body transformation and frames numbered three to six (^{18}F-FDG) or four to nine (^{18}F-DOPA) were averaged into one for further analysis.

Table 1 Subject characteristics and clinical data

Demographic and behavioural data: subjects with all imaging modalities				
	Healthy controls	**Parkinson's disease**	***P*-value**	**Test statistic**
n	14	42[a]	-	-
Gender male / female	7 / 7	26 / 16	0.43	$\chi^2 = 0.61$
Age, years	64.50 ± 8.29	67.24 ± 7.94	0.27	$t = 1.11$
MMSE	28.86 ± 1.03	28.36 ± 1.85	0.54	$W = 262$
Clinical characteristics: Parkinson's disease patients by subtype				
	Non-TD subtype	**TD subtype**	***P*-value**	**Test statistic**
n	39	3	-	-
Disease duration, years	4.49 ± 3.42	3.17 ± 2.36	0.71	$W = 66.5$
UPDRS III off Total score	24.49 ± 8.96	28.33 ± 3.79	0.21	$W = 32.5$
UPDRS III off AR score	10.51 ± 5.08	4.67 ± 0.58	0.03	$W = 103$
UPDRS III off Right body score	9.26 ± 4.22	11.67 ± 3.51	0.26	$W = 35$
UPDRS III off Left body score	9.23 ± 4.54	13.00 ± 5.00	0.18	$W = 30.5$
UPDRS III off Right body non-tremor score	8.41 ± 3.45	6.67 ± 2.08	0.31	$W = 79.5$
UPDRS III off Left body non-tremor score	8.36 ± 3.86	10.00 ± 4.36	0.46	$W = 43$
Hoehn and Yahr	2.31 ± 0.37	2.17 ± 0.29	0.59	$W = 69$
LEDD, mg	433.82 ± 236.45	401.67 ± 152.51	0.81	$W = 64$
$LEDD_A$, mg	127.37 ± 96.96	110.00 ± 127.67	0.77	$W = 65$
Side of onset L / R / equal	19 / 18 / 2	1 / 2 / 0	1[b]	$\chi^2 = 0.00$[b]

Clinical characteristics (mean ± SD) are summarized in the observed groups. Between-group differences were analysed using Mann-Whitney U-test, Student's *t*-test or in the case of dichotomous variables by χ^2 test.
[a]Only 42 because one subject did not undergo both PET acquisitions.
[b]Direct comparison of side-of-onset right versus side of onset left group in both subtypes using an approximate binominal test.
AR = akinetic-rigid; L = left; $LEDD_A$ = Levodopa equivalent daily dose for dopamine agonists; R = right; TD = tremor-dominant.

Averaged PET images were co-registered to the subject's blood oxygen level-dependent (BOLD)-weighted MRI data, stereotactically normalized by non-linear registration to an established ^{18}F-FDG (Della Rosa *et al.*, 2014) or ^{18}F-DOPA-PET template (García-Gómez *et al.*, 2013) in Montreal Neurological Institute (MNI) standard space and spatially filtered with a 6 mm full-width at half-maximum (FWHM) Gaussian smoothing kernel using SPM12 (www.fil.ion.ucl.ac.uk/spm/software/spm12).

A group comparison of ^{18}F-DOPA scans was conducted in SPM12 using the voxel-wise two sample *t*-test with default parameters (threshold masking, proportional scaling), applying a family-wise error (FWE) corrected peak-level threshold of $P < 0.05$, to define the study-specific location of most severe dopamine depletion in Parkinson's disease patients. The resulting clusters were saved as binary masks to enable cross-modality comparisons. These masks were later imported into the Conn toolbox (Whitfield-Gabrieli and Nieto-Castanon, 2012) and used as seed region of interest for evaluating how resting state functional connectivity is affected by dopamine depletion in striatal regions in Parkinson's disease patients. To assess individual regional ^{18}F-DOPA uptake, mean values were exported from significant clusters using the ROI SPM toolbox MarsBaR (Brett *et al.*, 2002).

The same procedure was followed to evaluate group differences in ^{18}F-FDG uptake. Following a whole-brain two-sample *t*-test, clusters where metabolism was significantly reduced in Parkinson's disease were saved as masks and normalized regional uptake values extracted for each subject and region of interest.

Resting state functional MRI

Acquisition of MRI data was performed on a 3.0 T Siemens Magnetom Prisma using the software system syngo MR D13D (Siemens). Acquisition parameters for T_1-weighted structural images were as follows: repetition time = 2300 ms, echo time = 2.32 ms, flip angle = 8°, field of view = 230 mm, slice thickness = 0.90 mm, voxel size = 0.9 × 0.9 × 0.9 mm, number of slices = 192. MRIs sensitive to changes in BOLD signal levels were obtained via a gradient-echo echo-planar imaging sequence (EPI) in interleaved acquisition mode. The slice thickness was 2 mm, field of view was 208 mm and the voxel size of functional data was 2.0 × 2.0 × 2.0 mm. Each brain volume comprised 72 axial slices, and each functional run contained 617 acquisition time points at a repetition time of 776 ms. Other technical parameters included echo time = 37.4 ms and flip angle = 55°.

All necessary preprocessing steps and resting state functional connectivity analysis of functional MRI data were performed using SPM12 and the SPM toolbox Conn v17 (Whitfield-

Gabrieli and Nieto-Castanon, 2017). The sequence of operations that was applied to co-registered structural and functional MRI data essentially followed the default preprocessing pipeline implemented in Conn. It included spatial realignment, outlier detection for correction of motion artefacts, direct segmentation and normalization to MNI space, spatial smoothing with a 5 mm FWHM 3D Gaussian filter, denoising [temporal band-pass filtering (0.01–0.1)], linear detrending and further reduction of physiological noise by anatomical component-based noise correction (aCompCor) (Behzadi *et al.*, 2007).

Resting state functional connectivity analysis

In seed-based resting state functional connectivity analysis, correlation coefficients were calculated between the mean time course of a predefined seed region of interest and the time course of all other voxels (or predefined target regions of interest) in a first-level analysis using bivariate correlation (Whitfield-Gabrieli and Nieto-Castanon, 2012). In the second-level analysis, correlation coefficients obtained in the first-level analysis were converted into normally distributed scores using Fisher's transformation. Fisher transformed correlation coefficients were included as dependent variables to test for statistically significant correlations between the seed region of interest and other voxels within groups, as well as to identify significant differences in connectivity between groups by performing *t*-tests. The threshold for significance was set to $P < 0.05$ FWE cluster-level corrected. In cortical regions where functional connectivity was altered in Parkinson's disease, individual seed-to-region of interest (ROI) correlation coefficients (β-values) were extracted for cross-modality analysis.

Cross-modality correlation analysis

Statistical analyses of cross-modality correlations were performed using R [R-project (R Core Team, 2018)]. Correlations between normalized regional ^{18}F-FDG and putaminal ^{18}F-DOPA uptake, ROI-to-ROI β-values, as well as between imaging modalities and clinical variables, were calculated using Pearson correlation. For between-group analysis and cross-modality correlation analysis only subjects who underwent all imaging modalities were included (Table 1). As dopaminergic and glucose metabolism are known to critically depend on age and functional connectivity is influenced by dopaminergic medication (Tahmasian *et al.*, 2015*a*), even in the OFF state, age and LEDD were included as covariates in partial correlation analyses. Additionally, correlations with motor scores were corrected for MMSE and vice versa to separately assess the influence of motor and cognitive symptoms. We distinguished between tremor-dominant and non-tremor-dominant patients when performing correlations with UPDRS-III ratings and subscores. As indicated in corresponding figures, results were considered significant for $P < 0.05$.

Data availability

The dataset generated and analysed during the present study will be made available from the corresponding author on reasonable request.

Results

Subject characteristics

In total, 42 patients with Parkinson's disease (67.24 ± 7.94 years old, 26 males) and 14 healthy controls (64.50 ± 8.29 years old, seven males) were available for all imaging modalities; hence only these were considered for clarifying associations between modalities (see Table 1 for clinical and demographic data). Only three of the patients with Parkinson's disease were classified as tremor-dominant. Tremor-dominant patients scored on average 28.33 ± 3.79 on the UPDRS-III and the mean Hoehn and Yahr score was 2.17 ± 0.29. Non-tremor-dominant patients scored 24.49 ± 8.96 on the UPDRS-III and the mean Hoehn and Yahr score was 2.31 ± 0.37. Left versus right side of onset was equally distributed in the present cohort. All participating Parkinson's disease patients received dopaminergic medication. Corresponding data for all subjects can be found in Supplementary Table 1.

Nigral hypometabolism and concomitant putaminal dopamine depletion

Voxel-wise group comparison of cerebral ^{18}F-FDG uptake in patients with Parkinson's disease and healthy controls revealed three clusters of regional hypometabolism in patients ($P < 0.05$ FWE cluster-level corrected). Activity was reduced in a cortical cluster that primarily comprised parts of the bilateral occipital fusiform gyri, inferior lateral occipital cortex and superior lateral occipital cortex (MNI coordinates: 26,–90,–10, $P < 0.001$ FWE cluster-level corrected; Fig. 1A and Table 2). On the left hemisphere, hypometabolism expanded into the posterior middle temporal gyrus (MNI coordinates: –66,–44,–4, $P = 0.019$ FWE cluster-level corrected; Fig. 1A and Table 2).

Aside from regions mentioned in the Parkinson's disease-related pattern, Parkinson's disease patients also exhibited significantly reduced ^{18}F-FDG metabolism in the midbrain (MNI coordinates: –10,–20,–20, $P < 0.001$ FWE cluster-level corrected; Fig. 1A, B and Table 2), which has never been reported in another Parkinson's disease cohort. The midbrain cluster included the left lateral caudal SNpc as identified with a probabilistic human *in vivo* atlas (Pauli *et al.*, 2018). This finding was also mentioned in a separate study by our group, which analysed the same PET dataset in a different context (Glaab *et al.*, 2019).

Nigrostriatal fibre degeneration and consequential reduction of dopaminergic terminals typically first and most severely affect the posterior putamen in Parkinson's disease (Kish *et al.*, 1988). In terms of network degeneration, reduced dopaminergic transmission can be understood as the second stage at which the neurodegenerative process can be assessed by functional brain imaging. ^{18}F-DOPA PET scans were used to determine the exact location and

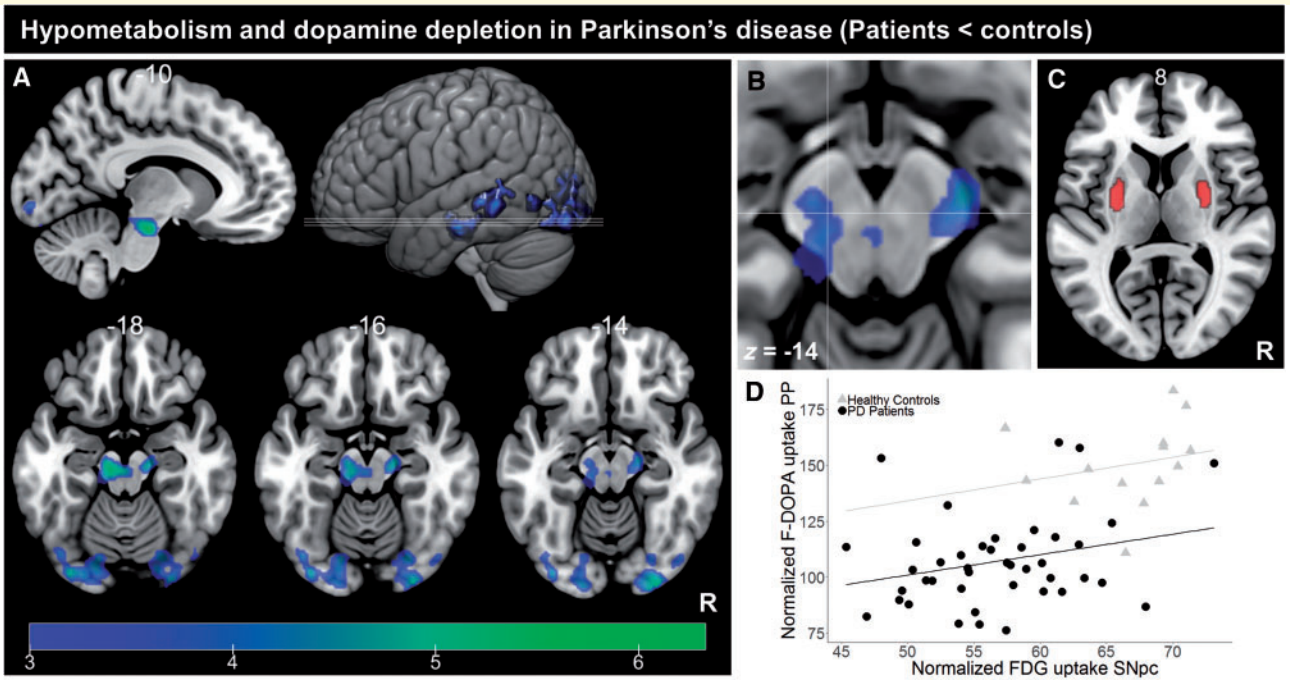

Figure 1 Between-group differences in F^{18}-FDG metabolism and ^{18}F-DOPA uptake. (**A**) Parkinson's disease patients exhibited a significantly reduced ^{18}F-FDG metabolism in a midbrain cluster spanning the lateral caudal part of the SN as well as in the bilateral occipital and left temporal cortex (FWE cluster level-corrected $P < 0.05$). Cortical regions that showed significant hypometabolism included the right and left occipital fusiform gyri (r OFusG, l OFusG), the right and left inferior occipital gyri (l iLOC, r iLOC) and the left middle temporal gyrus (pMTG). Colour bar indicates T-values and number on slices represent z-coordinates for axial slices or *x*-coordinates for sagittal slices. (**B**) Detailed display of the hypometabolic midbrain cluster, overlaid on anatomical MNI152 template. Crosshairs indicate the MNI coordinates: –10, –20, –14. (**C**) Spatial distribution of voxels exhibiting between-group differences in ^{18}F-DOPA uptake overlaid on the MNI152 template. Parkinson's disease patients showed significantly reduced dopamine synthesis capacity in the bilateral posterior putamen (PP) (FWE-peak-level-corrected $P < 0.001$). (**D**) Partial correlation analysis between nigral ^{18}F-FDG metabolism (*left*) and ipsilateral putaminal ^{18}F-DOPA uptake. A significant correlation was observed between normalized nigral metabolic activity (*left*) and ipsilateral, normalized putaminal ^{18}F-DOPA uptake in patients (Pearson correlation: r = 0.31, $P = 0.041$ corrected for age and LEDD), but not in healthy controls (r = 0.25, $P = 0.383$, corrected for age). PD = Parkinson's disease.

extent of reduced dopaminergic projections in the present cohort by whole-brain group comparison. ^{18}F-DOPA uptake was significantly reduced in the bilateral putamen in Parkinson's disease patients (MNI coordinates: –30, –10, 0 and 28, –6, 2, $P < 0.001$ FWE-peak-level corrected; Fig. 1C and Table 3). Both clusters were found to be mainly restricted to the posterior putamen when overlaid on an MNI152 structural template (Fig. 1C), using the anterior commissure as the antero-posterior border as suggested by Helmich *et al.* (2010). Dopamine depletion was asymmetrical in the current study cohort, with the left hemisphere being more affected (Table 3).

The relation between observed metabolic changes in the SNpc and putaminal dopamine depletion was analysed to verify the association between degenerative processes along the nigrostriatal pathway in patients with Parkinson's disease. Normalized ^{18}F-FDG uptake values exported from the nigral cluster, where patients exhibited the most significantly reduced metabolism ($P < 0.05$ FWE peak level correction), showed a significant positive correlation with normalized ^{18}F-DOPA uptake values of putaminal peak coordinates in patients with Parkinson's disease (r = 0.31, $P = 0.041$; Fig. 1D) when corrected for age and LEDD, but not in healthy controls (r = 0.25, $P = 0.383$; Fig. 1D). This linear relation between the most significant PET findings indicated that putaminal ^{18}F-DOPA uptake drops with decreasing nigral ^{18}F-FDG accumulation. Interestingly, both cerebral pathologies were primarily left-sided, with more profoundly reduced ^{18}F-FDG uptake in the left midbrain (Fig. 1B) and higher dopamine depletion in the left putamen (Fig. 1C and Table 3), suggesting a similarly asymmetrical pathology in SNpc and striatum.

Nigrostriatal pathway disruption was further analysed with ROI-to-ROI resting state functional connectivity between the midbrain cluster, in which patients with Parkinson's disease showed significantly reduced ^{18}F-FDG metabolism and putaminal clusters where dopamine deficiency was most severe. Functional connectivity was significantly reduced between the hypometabolic SNpc cluster and the bilateral posterior putamen region of interest in patients compared to healthy controls [$P = 0.043$ false-discovery-rate (FDR)-seed-level corrected; Supplementary

Table 2 Hypometabolic clusters in Parkinson's disease patients (FWE cluster level $P < 0.05$)

Region	Side	Size, voxel	x	y	z	T-value	FWE-corrected P-value
Brainstem	Left, right	455	−10	−20	−20	6.33	<0.001
OFusG	Left, right	2058	26	−90	−10	5.82	<0.001
iLOC	Left, right						
sLOC	Right						
pMTG	Left	188	−66	−44	−4	5.40	0.019

Height threshold = 3.25, extent threshold = 180 voxels
iLOG = inferior lateral occipital cortex; L = left; OFusG = occipital fusiform gyrus; pMTG = posterior middle temporal gyrus; R = right; sLOC = superior lateral occipital cortex.

Table 3 Dopamine depleted clusters in patients with Parkinson's disease

Region	Hemisphere	Size, voxels	x	y	z	T-value	FWE-corrected P-value
Putamen	Left	302	−30	−10	0	7.82	<0.001
Putamen	Right	204	28	−6	2	6.83	<0.001

Height threshold = 5.1
Characteristics of clusters in which patients exhibited significantly reduced putaminal ^{18}F-DOPA uptake.

Table 2]. These findings were validated in the same cohort with atlas-defined regions of interest, using the putamen and brainstem masks included in the Conn toolbox (FSL Harvard-Oxford atlas). When the predefined brainstem region of interest was used as seed mask, significantly reduced connectivity was evident between the brainstem and the right putamen ($P = 0.011$ FDR-seed-level corrected; Supplementary Table 2) as well as between the brainstem and both unilateral or bilateral cohort-specific posterior putaminal target regions of interest in patients compared to controls (posterior putamen left: $P = 0.019$, posterior putamen right: $P = 0.003$, posterior putamen bilateral: $P = 0.003$; Supplementary Table 2).

Putaminal resting state functional connectivity networks in healthy controls and Parkinson's disease patients

The study-specific bilateral posterior putamen cluster (Fig. 1C) was used as the seed region of interest for striatocortical functional connectivity analysis. Seed-to-voxel connectivity was first assessed separately in healthy controls and Parkinson's disease patients in a one sample *t*-test. In both groups, significant correlations of BOLD signal fluctuations were found between the bilateral putaminal seed region of interest and regions primarily belonging to the sensorimotor network, including the precentral gyrus, supplementary motor area, cerebellum, postcentral gyrus and parts of the parietal association cortex (Fig. 2 and Supplementary Tables 3 and 4). Visual comparison of patients' and controls' putaminal connectivity networks suggested several group differences (*cf.* Fig. 2A and B), e.g. functional correlation between the posterior putamen seed region of interest and the precentral gyrus appeared lower in Parkinson's disease. Interestingly, the bilateral putaminal seed was functionally correlated with larger parts of the cerebellum, primarily the anterior cerebellar lobe, in Parkinson's disease patients (bilateral cerebellar lobules 4–6: patients: 1681 voxels; controls: 479 + 520 voxels; Fig. 2A, B and Supplementary Tables 3 and 4).

Striatocortical hypoconnectivity is accompanied by reduced cortical metabolism

Between-group analysis of seed-to-voxel resting state functional connectivity networks was performed using bilateral or unilateral ^{18}F-DOPA-defined seed regions of interest and a two-sample *t*-test (patients < controls, $P < 0.05$ cluster-level FWE-corrected). Patients with Parkinson's disease exhibited significantly less functional connectivity between the dopamine depleted bilateral posterior putamen and several sensorimotor areas (Fig. 2C and Table 4). Cortical regions with reduced connectivity were identified using the Harvard-Oxford atlas. They primarily included the precentral gyrus, supplementary motor area, superior frontal gyrus and large clusters in the bilateral inferior parietal cortex (IPC), comprising the anterior and posterior part of the supramarginal gyrus as well as the neighbouring left and right opercular cortices (Fig. 2C and Table 4). Additionally, putaminal hypoconnectivity was detected in the bilateral precuneus, a central node of the DMN, and the brainstem. Interestingly, regardless of seed region of interest lateralization the most striking effects of reduced functional connectivity were located on the left cortical hemisphere and more severely when focusing on the left putamen (not shown). However, between-seed contrasts

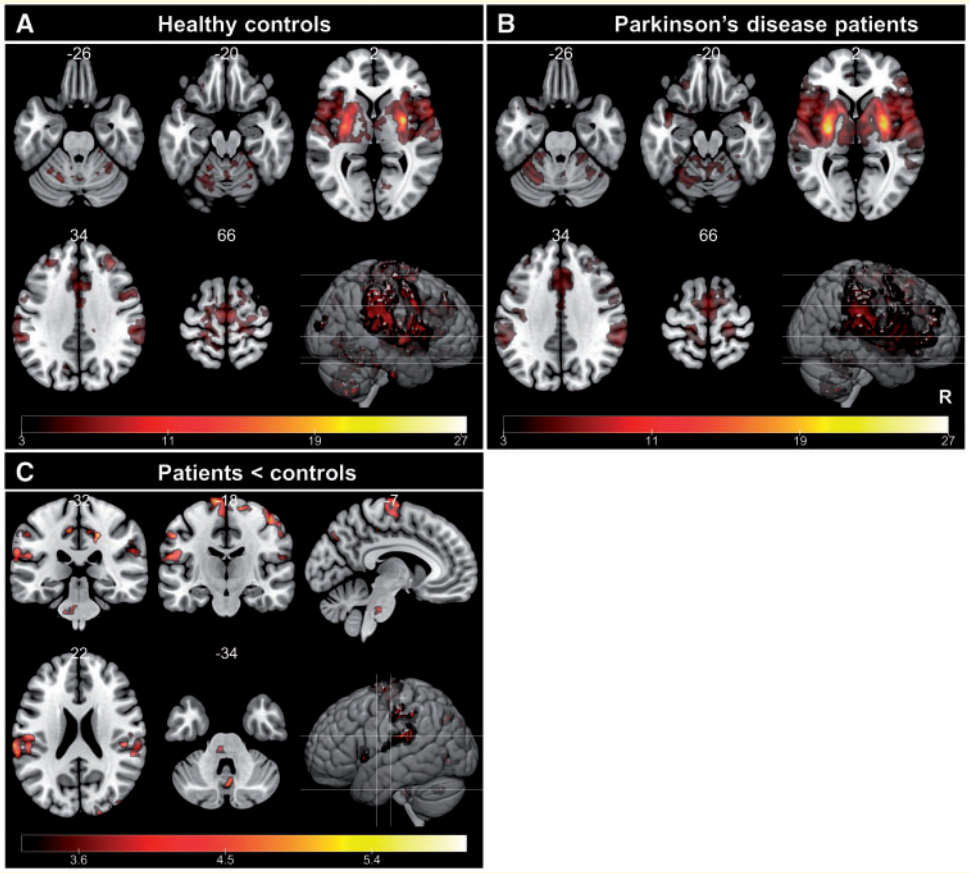

Figure 2 Dopamine depleted putaminal regions exhibit reduced functional synchrony with the sensorimotor network in patients with Parkinson's disease. Spatial distribution of clusters exhibiting significant correlations with the BOLD signal of the putaminal seed region of interest, in which dopamine depletion was most severe in Parkinson's disease patients, overlaid on T_1 MNI152 anatomical template. Red-yellow clusters indicate significant correlations with the BOLD signal of the posterior putamen (PP) in (**A**) healthy controls or (**B**) Parkinson's disease patients. (**C**) Spatial distribution of clusters in which patients exhibited a significantly reduced correlation with the posterior putamen seed region of interest compared to healthy controls. All results were corrected for multiple comparison, thresholded at $P < 0.05$ FWE cluster-level correction. Colour bar indicates corresponding *t*-values. Slices and 3D display were constructed with MRIcroGL, neurological display.

did not reveal statistically significant differences. A suspected increase in functional connectivity between the posterior putamen and the anterior cerebellar cortex did not reach significance when putaminal hyperconnectivity was analysed in a seed-to-voxel analysis. Similar cortical regions were found to exhibit putaminal hypoconnectivity when between-group contrasts were calculated between the total of 60 patients and 25 control subjects.

To analyse whether striatocortical connectivity disruption influences cortical metabolic activity, we exported functional connectivity values and normalized ^{18}F-FDG uptake values from each cortical cluster, which exhibited reduced functional correlation with the bilateral posterior putamen seed region of interest in Parkinson's disease. Despite low spatial similarity between significantly hypometabolic regions and areas that were less functionally connected to the posterior putamen in patients with Parkinson's disease, significant associations were apparent between both imaging modalities (Fig. 3). Mean functional connectivity β-values and ^{18}F-FDG uptake in the right and the left IPC clusters showed a significant positive correlation in the Parkinson's disease group (IPC left: r = 0.35, $P = 0.021$, IPC right: r = 0.36, $P = 0.018$; Fig. 3A and B, corrected for age and LEDD), but not in controls, indicating concomitant changes in striatocortical functional connectivity and metabolic activity. In other clusters, which displayed significant hypoconnectivity to the posterior putamen in Parkinson's disease, no significant correlation between functional connectivity values and glucose metabolism was detected.

Cerebral pathologies traced by multimodal imaging reflect clinical impairment

As an association between more severe motor symptoms and functional network alterations was hypothesized, correlation analyses were performed between imaging findings and motor scores in non-tremor dominant patients.

Table 4 Between-group differences in putaminal functional connectivity (FWE-cluster-level corrected $P < 0.05$)

Region	Side	Size, voxel	x	y	z	T-value	FWE-corrected P-value
Precuneus	Right	135	20	–32	42	5.98	0.001
PC	Right						
PreCG	Left / right	840	–4	–10	72	5.54	<0.001
SFG	Left						
SMA	Left						
LG	Right	81	10	–76	–6	5.36	0.02
CO	Left	608	–68	–26	22	5.30	<0.001
PO	Left						
aSMG	Left						
PostCG	Left						
PreCG	Right	549	44	–18	56	5.28	<0.001
PostCG	Right						
PostCG	Left	306	–54	–20	40	5.23	<0.001
aSMG	Left						
PreCG	Right	92	4	–24	50	5.02	0.010
PO	Right	381	46	–26	22	4.82	<0.001
aSMG	Right						
PT	Right						
pSMG	Right						
OP	Right	200	22	–96	24	4.65	<0.001
sLOC	Right						
IFG oper	Left	83	–48	12	6	4.51	0.018
Precuneus	Left	104	–10	–72	38	4.49	0.005
Brainstem	Left / right	69	–2	–34	–32	4.47	0.044

All *t*-values were calculated using Conn in SPM12, significance was thresholded at $P < 0.05$ FWE-corrected at cluster-level. Extent threshold $k = 69$ voxels, height threshold T = 3.25. aSMG = anterior supramarginal gyrus; CO = central operculum cortex; IFG oper = inferior frontal gyrus pars opercularis; LG = lingual gyrus; OP = occipital pole; PC = cingulate gyrus; posterior; PO = parietal operculum cortex; PostCG = postcentral gyrus; PreCG = precentral gyrus; pSMG = posterior supramarginal gyrus; PT = planum temporale; SFG = superior frontal gyrus; sLOC = superior lateral occipital cortex; SMA = supplementary motor area.

Interestingly, the degree of side-specific akinetic-rigid symptoms, quantified by UPDRS-III right body non-tremor score, negatively correlated with metabolic activity in the left SNpc, suggesting a relation between decreasing ^{18}F-FDG uptake in degenerating midbrain structures and akinesia-rigidity in Parkinson's disease (Fig. 4A, r = –0.40, $P = 0.010$). Focusing on disease duration, significantly reduced midbrain metabolism was observed in patients with a disease duration >7 years compared to patients with a disease duration of ⩽7 years ($P = 0.016$, Welch-test, one-sided). Predictably, right body akinesia and rigidity was accompanied by more severe dopaminergic deficits in the left putamen as quantified by ^{18}F-DOPA-PET (Fig. 4B, r = –0.38, $P = 0.014$). Nigrostriatal functional connectivity between the midbrain and bilateral posterior putamen negatively correlated with non-tremor-dominant patients' total akinesia-rigidity scores (Fig. 4C, r = –0.49, $P = 0.0008$). Interestingly, a negative linear trend was observed between UPDRS-III right body scores and β-values quantifying the degree of connectivity between the left posterior putamen seed region of interest and the left IPC cluster (coordinates –68,–26, 22), which was one of the cortical regions exhibiting less functional correlation with the posterior putamen in patients (Fig. 4D, r = –0.31, $P = 0.053$, corrected for age, LEDD and MMSE). In other cortical clusters, including motor regions, which showed putaminal dysconnectivity, no significant correlation between functional connectivity values and motor impairment could be observed. In addition, the left hypoconnected IPC cluster was the only cortical region in which normalized ^{18}F-FDG uptake exhibited a negative linear trend with contralateral motor impairment (Fig. 4E, r = –0.31, $P = 0.057$, corrected for age, LEDD, MMSE and disease duration). Further, in the left IPC a positive correlation between total cognition MMSE score and striatocortical connectivity values was observed in patients with Parkinson's disease (Fig. 4E, r = 0.42, $P = 0.005$, corrected for age, LEDD, and akinesia-rigidity-score).

Discussion

The current study opens new perspectives by being the first to assess network degeneration in patients with Parkinson's disease by using a multimodal imaging approach in a large cohort of patients. Combining functional imaging methods has been a useful method to describe the vulnerability of distinct networks for neurodegenerative processes, but to

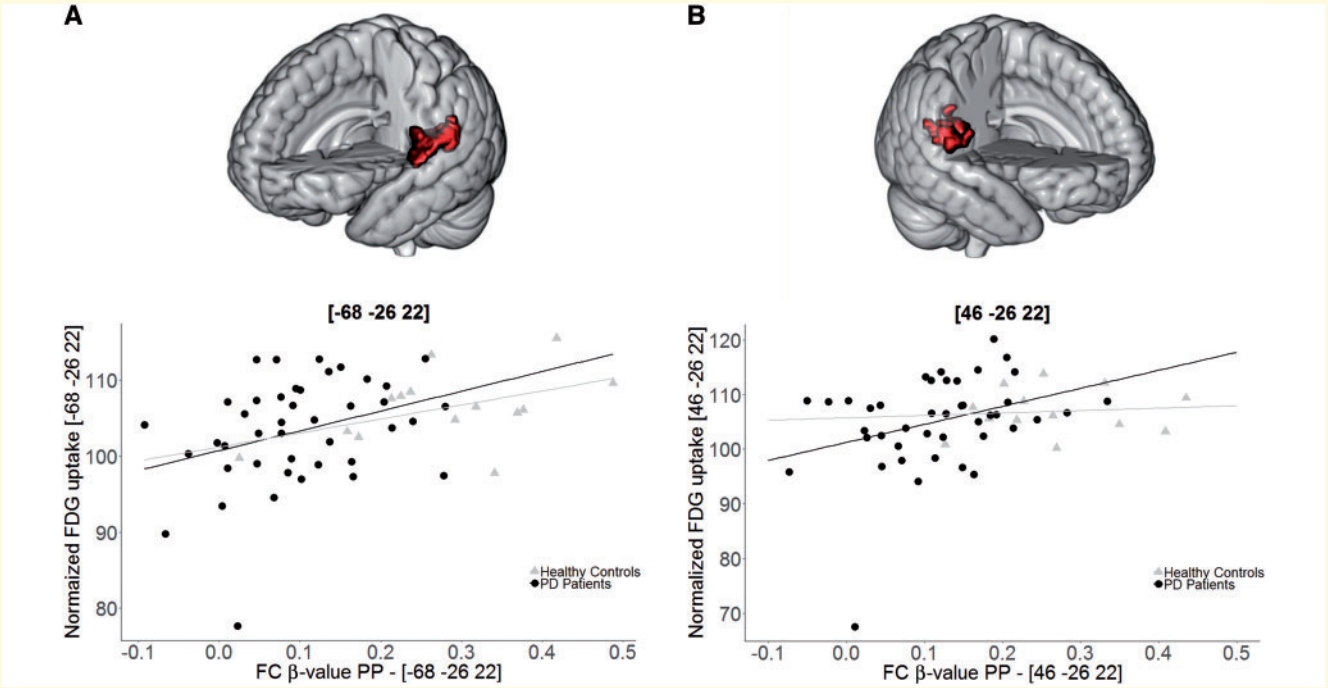

Figure 3 Striatocortical connectivity β-values correlate with metabolic activity in the bilateral inferior parietal cortex in patients with Parkinson's disease. Correlation analysis between subject-specific functional connectivity β-values, characterizing the connection between the posterior putamen (PP) seed region of interest and the (**A**) IPC left (r = 0.35, *P* = 0.021) or (**B**) IPC right (r = 0.36, *P* = 0.018) cluster, which were both less functionally correlated with the posterior putamen in Parkinson's disease patients, and normalized ^{18}F-FDG-PET values exported from respective cortical clusters. In healthy controls both correlations revealed no significant results [IPC left (r = 0.47, *P* = 0.079), IPC right (r = 0.36, *P* = 0.237)]. All correlation analyses were corrected for age and in patients also for LEDD. PD = Parkinson's disease.

date not for Parkinson's disease. In patients with Parkinson's disease, specific cortico–subcortical functional and metabolic changes have been described previously, but many studies were restricted to one or two imaging modalities, limiting cross-modality insights that could improve the understanding of disease pathology on a network level. We combined three functional imaging modalities, including ^{18}F-DOPA-PET, ^{18}F-FDG-PET and functional MRI to characterize functional consequences of cerebral pathologies and their regional association in patients with Parkinson's disease in comparison to healthy subjects. In summary, results support the hypothesis that degeneration of nigrostriatal connections and its neurochemical consequences in Parkinson's disease impair functional activity in specific cortical regions with strong association to motoric function. Using high-resolution PET data, we were the first to detect hypometabolism in the SNpc of patients with Parkinson's disease. This was accompanied by reduced nigrostriatal connectivity and dopamine depletion, which in turn appeared to cause a disruption in striatocortical resting state functional connectivity. Putaminal dysconnectivity in patients primarily affected the sensorimotor network and regions deploying the DMN. More severe functional desynchronization with the striatum was also accompanied by decreased global cognitive performance and lower neural activity in the IPC in patients, suggesting that reduced input from the striatum leads to concomitant metabolic changes in the cerebral cortex and potentially cognitive decline.

In vivo detection of nigrostriatal pathway disruption

The hypometabolic cortical areas observed in the current study stand in accordance with previous studies that reported reduced metabolic activity in parieto-occipital regions in Parkinson's disease (Eidelberg, 2009; Teune *et al.*, 2010; Granert *et al.*, 2015). The observed hypometabolic midbrain cluster overlapped in parts with the lateral and caudal SNpc, as confirmed by a high-resolution subcortical nuclei atlas (Pauli *et al.*, 2018), in correspondence with regions where nigral cell bodies are known to degenerate first. The significantly reduced metabolism observed in patients with Parkinson's disease might reflect an indirect correlate of severe loss of neural cell bodies which contribute to the nigrostriatal pathway, a major neuropathological hallmark of Parkinson's disease that has already been described *in vivo* in Parkinson's disease and rapid eye movement (REM) sleep behaviour disorder (RBD) patients using different MRI techniques (Ohtsuka *et al.*, 2013;

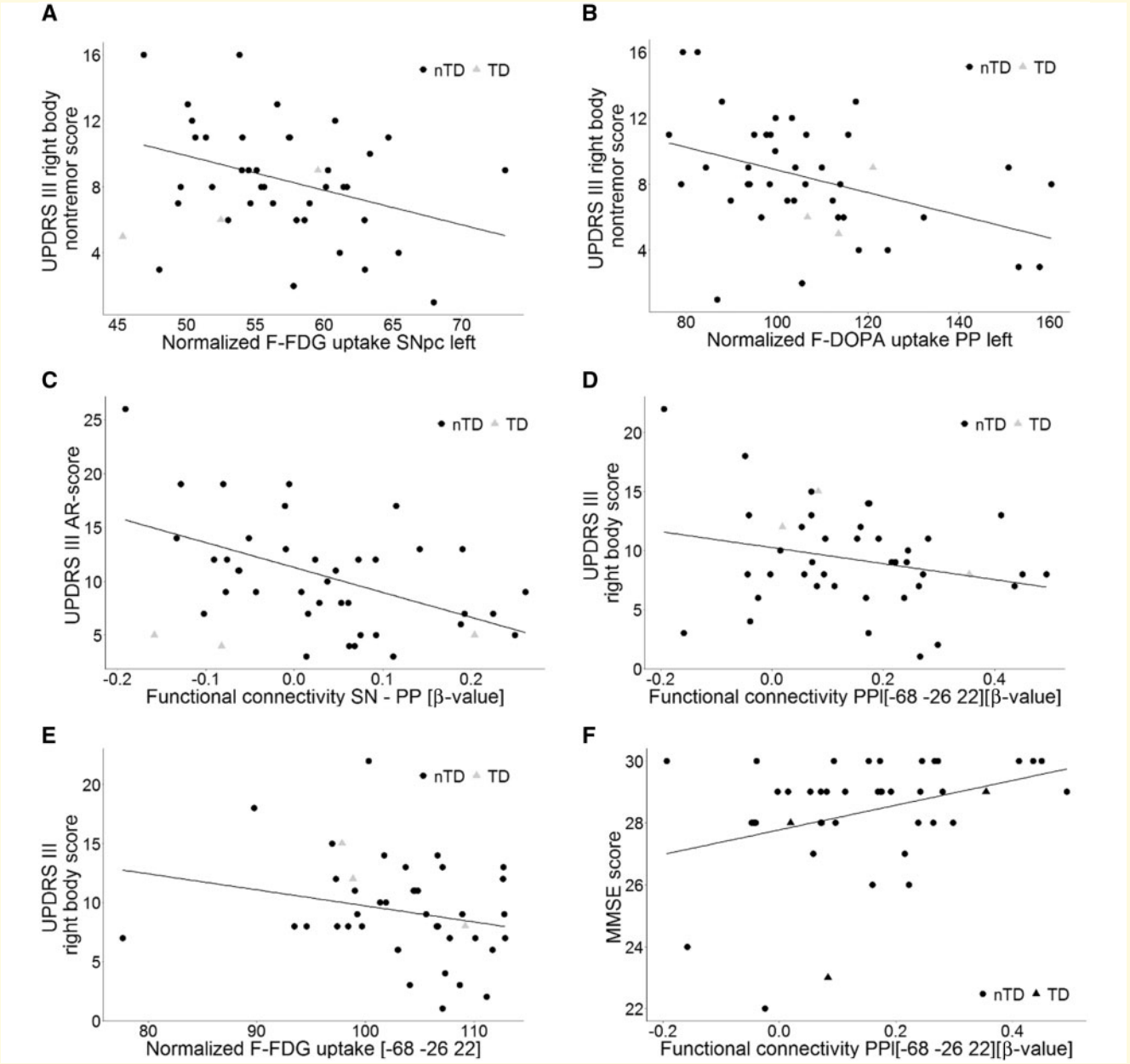

Figure 4 Multimodally assessed nigrostriatal pathway integrity and functional alterations in the IPC correspond with motor and cognitive impairments in patients with Parkinson's disease. Partial correlation analyses between subject-specific UPDRS-III right body non-tremor scores and (**A**) nigral metabolism (*left*) ($r = -0.40$, $P = 0.010$), (**B**) putaminal ^{18}F-DOPA uptake (*left*) ($r = -0.38$, $P = 0.014$), (**C**) functional connectivity between SNpc and posterior putamen (PP) and UPDRS-III akinesia-rigidity score ($r = -0.49$, $P < 0.001$), UPDRS-III right body scores and (**D**) β-values quantifying functional connectivity between the posterior putamen left (PPl) seed and left IPC cluster (peak coordinates: –68, –26, 22) ($r = -0.31$, $P = 0.053$), or (**E**) normalized ^{18}F-FDG uptake in the left IPC cluster quantified by ^{18}F-FDG-PET in non-tremor-dominant patients ($r = -0.31$, $P = 0.057$). (**F**) Global cognition score on MMSE and β-values quantifying functional connectivity between the PPl seed and left IPC cluster in all patients (peak coordinates: –68 –26 22) ($r = 0.42$, $P = 0.005$). All correlations were corrected for age and LEDD and in the case of (**D**) MMSE, (**E**) MMSE, disease duration and (**F**) akinesia-rigidity (AR) scores were included as additional covariates. UPDRS-III right body non-tremor scores (maximum: 24), right body scores (maximum: 36) and akinesia-rigidity scores (maximum = 48) were calculated, as provided in the Supplementary material.

Pyatigorskaya *et al.*, 2017). Using neuromelanin-sensitive MRI, Ohtsuka *et al.* (2013) observed cell death-associated depigmentation in the lateral SNpc in Parkinson's disease, where hypometabolism was evident in our patients. Both findings stand in accordance with topography of dopaminergic cell loss, most strongly affecting the caudal and mediolateral part of the SNpc, histopathologically described by Damier *et al.* (1999). Dopaminergic neurons in the SNpc

have been characterized as highly energy consuming neurons with numerous mitochondria, poor myelination, and long axonal processes, which makes them especially vulnerable to exhaustion (Braak *et al.*, 2006; Seibyl *et al.*, 2012). In consideration of the devastating decline of nigral neurons, which is already evident when first motor symptoms occur, the observed hypometabolic cluster is likely to reflect secondary metabolic changes due to the loss of high energy consuming neural populations. Despite this pathophysiological knowledge, nigral hypometabolism in human patients with Parkinson's disease has not been previously described, probably because resolution was lower than of the HRRT-PET scanner in the current study or because of smaller sample sizes.

To date, similar results were only reported in a 6-hydroxydopamine-lesioned rat model using high-resolution small-animal ^{18}F-FDG-PET, where the strongest metabolic impairment was seen in the SNpc, attributable to dopaminergic cell loss (Jang *et al.*, 2012). Notably, we previously observed increased metabolic activity in the substantia nigra in an early-stage Parkinson's disease cohort of 10 patients (five unmedicated) with high resolution PET (Eggers *et al.*, 2009). In the latter study a different, region of interest-based approach was applied with nigral regions of interest drawn manually in native space. However, early-stage nigral hypermetabolism could reflect inflammatory processes, which may initially outweigh reduced neural metabolism due to neurodegeneration (Gerhard *et al.*, 2006; de Virgilio *et al.*, 2016). Evidence for a disease-stage dependent process is given in the linear relationship between midbrain metabolism and contralateral disease severity and the fact that stronger metabolic deficits in the midbrain were observed in patients with longer disease duration. It is noteworthy that several studies report an increased metabolism in pontine regions (Niethammer and Eidelberg, 2012; Granert *et al.*, 2015), which might 'blur over' reduced metabolism in the caudal midbrain on lower resolution scanners.

In the current study, a modest linear correlation between unilateral nigral ^{18}F-FDG uptake and ipsilateral putaminal ^{18}F-DOPA uptake was observed, suggesting a linear association between detected abnormalities identified along nigrostriatal connections. The correlation was relatively low, which may be due to a 'floor effect', meaning that in patients with more advanced degeneration, nigral ^{18}F-FDG activity and/or fluorodopa uptake in the posterior putamen would have reached a minimum; or varying degrees of inflammatory activity between patients, which could not be distinguished from neural activity using ^{18}F-FDG-PET. The description of concomitant changes was supported by resting state functional MRI findings, which implied that pathological changes are directly related to impaired functional coherence between the hypometabolic midbrain and dopamine depleted putamen, an observation underpinned by comparable studies (Sharman *et al.*, 2013). In conclusion, corresponding deficits along the nigrostriatal pathway were identified *in vivo* by measuring correlates of neural dysfunction (^{18}F-FDG), dopaminergic activity (^{18}F-DOPA-PET) and functional synchrony (resting state functional MRI). Of note, cerebral pathologies identified along this pathway corresponded with contralateral akinetic-rigid symptoms, suggesting an involvement in motor impairment.

Striatocortical functional network degeneration and metabolic consequences

In accordance with previous assumptions, the distribution of connectivity disruption in patients with Parkinson's disease converged with spatial patterns of putaminal functional connectivity networks in controls, indicating functional motor network disturbances in Parkinson's disease. These findings are consistent with anatomical studies pointing out parallel functional loops of different putaminal subregions in non-human primates (Alexander *et al.*, 1986) and functional imaging studies that emphasize functionally segregated striatocortical circuits in humans (Postuma and Dagher, 2006; Di Martino *et al.*, 2008; Helmich *et al.*, 2010). Although functional connectivity does not necessarily reflect direct anatomical connections, the current findings mostly overlap with structural putaminal connectivity networks and therefore are likely to reflect correlates of spatially organized direct connections and their reduced functional integrity in Parkinson's disease (Postuma and Dagher, 2006; Cacciola *et al.*, 2017). Of note, significantly reduced functional connectivity was detected between the bilateral putaminal seed region of interest, where dopamine depletion was most severe in the present cohort, and cortical regions of the sensorimotor network, suggesting a putative role of putaminal dopaminergic dysfunction as conjoining element, through which pathology enters the cerebral cortex. These findings are suggestive of pathologic processes that target predefined neural networks. More precisely, attenuation of nigrostriatal transmission leads to dysfunctions within the striatocortical loop responsible for sensorimotor processing by provoking an imbalanced functional coherence between areas that exhibit strong functional correlation in healthy controls. In line with these findings, a topographic overlap between predominant subcortical atrophy identified by deformation-based morphometry in Parkinson's disease and intrinsic connectivity networks in healthy controls was previously reported, and the observed patterns were suggestive of an SN-centred pathogenic epicentre (Zeighami *et al.*, 2015). Yau *et al.* (2018) described longitudinally that cortical thinning in Parkinson's disease primarily affects regions with high connectivity to a 'disease reservoir', a set of subcortical regions affected at baseline (Zeighami *et al.*, 2015). Those observations emphasize that vulnerability of affected cortical areas is determined by their functional connection to previously damaged subcortical areas, and along with the current findings support the hypothesis of network-dependent degeneration in Parkinson's disease.

In the current study, significantly reduced resting state functional connectivity was evident between the posterior putamen and mainly the bilateral precentral gyrus and postcentral gyrus, supplementary motor area but also the IPC in patients with Parkinson's disease (Fig. 2). In line with the current findings, Helmich *et al.* (2010) also reported similar findings regarding putaminal hypoconnectivity in Parkinson's disease and asymptomatic leucine-rich repeat kinase 2 (LRRK2) mutation carriers (Helmich *et al.*, 2015). Furthermore, a quantitative neuroimaging meta-analysis provided evidence for disturbed functional connectivity of the bilateral IPC in Parkinson's disease (Tahmasian *et al.*, 2017). Additionally, in the current study, normalized ^{18}F-FDG uptake values exported from hypoconnected IPC clusters significantly correlated with β-values quantifying the degree of connectivity between the posterior putamen and the respective IPC cluster in patients (Fig. 3). Hypometabolism in the IPC has been reported as a promising predictive value for Parkinson's disease in a meta-analysis that examined sensitivity of ^{18}F-FDG-PET and structural atrophy, albeit that this phenomenon was mainly attributed to cognitive symptoms (Albrecht *et al.*, 2019).

Interestingly, the IPC is thought to represent the conjoining element in sensory feedback processing during movement tasks (Mattingley *et al.*, 1998), which is of great interest facing the association between contralateral motor impairments and the connectivity between the posterior putamen and the left IPC (Fig. 4D) as well as concomitant changes in glucose metabolism (Fig. 4E). In line with the latter findings, an important role of the IPC in sensorimotor processing and integration has been postulated (Wang *et al.*, 2017). The IPC represents the intersection of several networks (DMN, ventral attention, frontoparieral control network, sensorimotor), rather than a component of a single network with specialized function. From a broader point of view, the IPC might represent the missing link between motor and cognitive deficits in Parkinson's disease. The identified IPC clusters encompass areas responsible for sensorimotor processing and default mode activity, according to functional subdivisions defined by Wang *et al.* (2017) and we observed a positive correlation between global cognition quantified by MMSE scores and the connectivity between the left IPC and posterior putamen. DMN dysfunction might arise secondarily to dopamine depletion (van Eimeren *et al.*, 2009; Wu *et al.*, 2012), more precisely in consequence of putaminal dysconnectivity of distinct DMN components, e.g. the IPC, which may provoke an impaired functional communication within the DMN and, eventually, cognitive decline. Additionally, cortical areas that exhibited putaminal dysconnectivity in patients could be related to non-motor symptoms as some of them, e.g. the superior frontal gyrus and fronto-insular network, were reported to be involved in impulsivity (Tahmasian *et al.*, 2015*b*; Schwartz *et al.*, 2019) and anosognosia in Parkinson's disease in previous studies (Maier *et al.*, 2016). Variability of the clinical course in different subtypes might partially depend on which non-motor networks are impaired and thereby determine susceptibility to non-motor symptoms.

Outlook and limitations

A relatively broad range of variability in medication and motor symptom severity is a typical limitation for a mild-to-moderately affected Parkinson's disease cohort.

As it has been suspected that levodopa attenuates radioligand binding (Politis, 2014), partially normalizes ^{18}F-FDG activity (Asanuma *et al.*, 2006), and alters resting state functional connectivity (Tahmasian *et al.*, 2015*a*), all functional image acquisitions were performed in the OFF state. Dopamine replacement therapy has been assumed to normalize functional connectivity alterations within the sensorimotor network and longer lasting effects of dopaminergic therapy on resting state functional MRI have been suggested (Tahmasian *et al.*, 2015*a*). This issue was partly addressed by incorporating LEDD as covariate in correlation analyses. However, as similar changes in putaminal resting state functional connectivity have been described in drug-naïve patients with Parkinson's disease, it can be assumed that residual medication-related effects seen in the OFF state are fairly small (Luo *et al.*, 2014). Further analysis should also focus on large scale networks, in relation to non-motor symptoms and dopamine depletion.

In consideration of residual inter-subject variability, an accurate detection of small subcortical nuclei like the SNpc is always afflicted with some uncertainty. Nonetheless, the identification of the SNpc using a probabilistic atlas of subcortical nuclei suggests a metabolic deficit due to loss of nigral neurons. If this observation is consistently reproduced using high-resolution PET acquisitions examining different disease stages, it would have diagnostic importance as a metabolic parameter with clinical relevance. Nonetheless, one limitation here is the lower number of controls, which was limited by the Federal Bureau for Radiation.

Finally, only indirect correlates of neurodegeneration were assessed. However, multimodal approaches and prospective availability of specific α-synuclein PET tracers may provide important additional insights into network degeneration and enable monitoring of disease progression. Measuring the degree of network degeneration at different stages, including subclinical network changes in prodromal subjects, could allow the identification of objectively definable disease stages.

Conclusion

The present findings suggest that in consequence of cellular degeneration, affecting vulnerable dopaminergic neurons within the SNpc, sequential functional alterations are initiated in Parkinson's disease. Network degeneration

seems to spread beyond nigrostriatal dopaminergic projections into cortical areas belonging to the sensorimotor network, including the bilateral precentral gyrus, supplementary motor area and the IPC, which has outstanding functions in sensorimotor integration and might represent the link between basal ganglia dysfunction and DMN alterations. To our knowledge this is the first study that shows midbrain hypometabolism in Parkinson's disease and combines ^{18}F-DOPA-PET, ^{18}F-FDG-PET and functional MRI to examine spatial associations between multimodally assessed pathologies. The unique multimodal approach applied in the current study successfully detected cerebral pathologies from decline of midbrain nuclei through putaminal dopamine depletion to striatocortical motor circuit dysfunction, which stands in accordance with the degree of motor disability in the patients analysed, highlighting the capability of multimodal imaging protocols as biomarkers, which may be suitable for quantification of disease progression.

Acknowledgements

We would like to thank all the participants who took part in the study and all of our colleagues who helped with data acquisition for their support in making the current research project possible.

Funding

This study received funding by the the German Research Association (DFG) in context of the Clinical Research Group 219 (KFO 219, EG350/1–1).

Competing interests

The authors report no competing interests.

Supplementary material

Supplementary material is available at *Brain* online.

References

Albin RL, Young AB, Penney JB. The functional anatomy of basal ganglia disorders. Trends Neurosci 1989; 12: 366–75.

Albrecht F, Ballarini T, Neumann J, Schroeter ML. FDG-PET hypometabolism is more sensitive than MRI atrophy in Parkinson's disease: a whole-brain multimodal imaging meta-analysis. Neuroimage Clin 2019; 21: 101594.

Alexander GE, DeLong MR, Strick PL. Parallel organization of functionally segregated circuits linking basal ganglia and cortex. Annu Rev Neurosci 1986; 9: 357–81.

Asanuma K, Tang C, Ma Y, Dhawan V, Mattis P, Edwards C, et al. Network modulation in the treatment of Parkinson's disease. Brain 2006; 129: 2667–78.

Behzadi Y, Restom K, Liau J, Liu TT. A component based noise correction method (CompCor) for BOLD and perfusion based fMRI. Neuroimage 2007; 37: 90–101.

Bischof GN, Ewers M, Franzmeier N, Grothe MJ, Hoenig M, Kocagoncu E, et al. Connectomics and molecular imaging in neurodegeneration. Eur J Nucl Med Mol Imaging 2019; 46: 2819–30.

Bischof GN, Jessen F, Fliessbach K, Dronse J, Hammes J, Neumaier B, et al. Impact of tau and amyloid burden on glucose metabolism in Alzheimer's disease. Ann Clin Transl Neurol 2016; 3: 934–9.

Braak H, Del Tredici K, Rüb U, de Vos R, Jansen Steur E, Braak E. Staging of brain pathology related to sporadic Parkinson's disease. Neurobiol Aging 2003; 24: 197–211.

Braak H, Rüb U, Schultz C, Del Tredici K. Vulnerability of cortical neurons to Alzheimer's and Parkinson's diseases. J Alzheimer's Dis 2006; 9: 35–44.

Brett M, Anton JL, Valabregue R, Poline J-B. Region of interest analysis using an SPM toolbox. In: Presented at the 8th International Conferance on Functional Mapping of the Human Brain, Sendai, Japan. 2002. Available on CD-ROM in NeuroImage, Vol 16, No 2. http://www.imm.dtu.dk/~fn/ps/Nielsen2002Translating_abstract.ps.gz.

Buckner RL, Sepulcre J, Talukdar T, Krienen FM, Liu H, Hedden T, et al. Cortical hubs revealed by intrinsic functional connectivity: mapping, assessment of stability, and relation to Alzheimer's disease. J Neurosci 2009; 29: 1860–73.

Buckner RL, Snyder AZ, Shannon BJ, LaRossa G, Sachs R, Fotenos AF, et al. Molecular, structural, and functional characterization of Alzheimer's disease: evidence for a relationship between default activity, amyloid, and memory. J Neurosci 2005; 25: 7709–17.

Cacciola A, Calamuneri A, Milardi D, Mormina E, Chillemi G, Marino S, et al. A connectomic analysis of the human basal ganglia network. Front Neuroanat 2017; 11: 85.

Cerasa A, Novellino F, Quattrone A. Connectivity changes in Parkinson's disease. Curr Neurol Neurosci Rep 2016; 16: 91.

Cope TE, Rittman T, Borchert RJ, Jones PS, Vatansever D, Allinson K, et al. Tau burden and the functional connectome in Alzheimer's disease and progressive supranuclear palsy. Brain 2018; 141: 550–67.

Damier P, Hirsch EC, Agid Y, Graybiel AM. The substantia nigra of the human brain. II. Patterns of loss of dopamine-containing neurons in Parkinson's disease. Brain 1999; 122 (Pt 8): 1437–48.

Della Rosa PA, Cerami C, Gallivanone F, Prestia A, Caroli A, Castiglioni I, et al. A standardized 18F-FDG-PET template for spatial normalization in statistical parametric mapping of dementia. Neuroinform 2014; 12: 575–93.

DeLong MR. Primate models of movement disorders of basal ganglia origin. Trends Neurosci 1990; 13: 281–5.

Di Martino A, Scheres A, Margulies DS, Kelly AMC, Uddin LQ, Shehzad Z, et al. Functional connectivity of human striatum: a resting state FMRI study. Cereb Cortex 2008; 18: 2735–47.

Dronse J, Fliessbach K, Bischof GN, von RB, Faber J, Hammes J, et al. In vivo patterns of tau pathology, amyloid-β burden, and neuronal dysfunction in clinical variants of Alzheimer's disease. J Alzheimers Dis 2017; 55: 465–71.

Drzezga A. The network degeneration hypothesis: spread of neurodegenerative patterns along neuronal brain networks. J Nucl Med 2018; 59: 1645–8.

Drzezga A, Becker JA, van Dijk KRA, Sreenivasan A, Talukdar T, Sullivan C, et al. Neuronal dysfunction and disconnection of cortical hubs in non-demented subjects with elevated amyloid burden. Brain 2011; 134: 1635–46.

Eggers C, Hilker R, Burghaus L, Schumacher B, Heiss WD. High resolution positron emission tomography demonstrates basal ganglia dysfunction in early Parkinson's disease. J Neurol Sci 2009; 276: 27–30.

Eggers C, Kahraman D, Fink GR, Schmidt M, Timmermann L. Akinetic-rigid and tremor-dominant Parkinson's disease patients show different patterns of FP-CIT single photon emission computed tomography. Mov Disord 2011; 26: 416–23.

Ehgoetz Martens KA, Hall JM, Georgiades MJ, Gilat M, Walton CC, Matar E, et al. The functional network signature of heterogeneity in freezing of gait. Brain 2018; 141: 1145–60.
Eidelberg D. Metabolic brain networks in neurodegenerative disorders: a functional imaging approach. Trends Neurosci 2009; 32: 548–57.
Emre M, Aarsland D, Brown R, Burn DJ, Duyckaerts C, Mizuno Y, et al. Clinical diagnostic criteria for dementia associated with Parkinson's disease. Mov Disord 2007; 22: 1689–707. quiz 1837.
Fahn S, Elton RL. UPDRS development committee. The unified Parkinson's disease rating scale. In: Fahn S, Marsden CD, Calne DB, Goldstein M, editors. Recent developments in Parkinson's disease. 2nd edn. Florham Park, NJ: Macmillan Healthcare Information; 1987. p. 153–63. p. 293–304.
Folstein MF, Folstein SE, McHugh PR. "Mini-mental state". J Psychiatric Res 1975; 12: 189–98.
García-Gómez FJ, García-Solís D, Luis-Simón FJ, Marín-Oyaga VA, Carrillo F, Mir P, et al. Elaboración de una plantilla de SPM para la normalización de imágenes de SPECT con 123I-Ioflupano. Rev Espanola Med Nucl Imagen Mol 2013; 32: 350–6.
Gerhard A, Pavese N, Hotton G, Turkheimer F, Es M, Hammers A, et al. In vivo imaging of microglial activation with 11C(R)-PK11195 PET in idiopathic Parkinson's disease. Neurobiol Dis 2006; 21: 404–12.
Ghasemi M, Mahloojifar A. Disorganization of equilibrium directional interactions in the brain motor network of Parkinson's disease: new insight of resting state analysis using granger causality and graphical approach. J Med Signals Sens 2013; 3: 69–78.
Glaab E, Trezzi J-P, Greuel A, Jäger C, Hodak Z, Drzezga A, et al. Integrative analysis of blood metabolomics and PET brain neuroimaging data for Parkinson's disease. Neurobiol Dis 2019; 124: 555–62.
Granert O, Drzezga AE, Boecker H, Perneczky R, Kurz A, Götz J, et al. Metabolic topology of neurodegenerative disorders: influence of cognitive and motor deficits. J Nucl Med 2015; 56: 1916–21.
Hacker CD, Perlmutter JS, Criswell SR, Ances BM, Snyder AZ. Resting state functional connectivity of the striatum in Parkinson's disease. Brain 2012; 135: 3699–711.
Helmich RC, Derikx LC, Bakker M, Scheeringa R, Bloem BR, Toni I. Spatial remapping of cortico-striatal connectivity in Parkinson's disease. Cereb Cortex 2010; 20: 1175–86.
Helmich RC, Thaler A, van Nuenen BFL, Gurevich T, Mirelman A, Marder KS, et al. Reorganization of corticostriatal circuits in healthy G2019S LRRK2 carriers. Neurology 2015; 84: 399–406.
Hoehn MM, Yahr MD. Parkinsonism: onset, progression and mortality. Neurology 1967; 17: 427–42.
Hoenig MC, Bischof GN, Seemiller J, Hammes J, Kukolja J, Onur ÖA, et al. Networks of tau distribution in Alzheimer's disease. Brain 2018; 141: 568–81.
Jang DP, Min H-K, Lee S-Y, Kim IY, Park HW, Im YH, et al. Functional neuroimaging of the 6-OHDA lesion rat model of Parkinson's disease. Neurosci Lett 2012; 513: 187–92.
Kish SJ, Shannak K, Hornykiewicz O. Uneven pattern of dopamine loss in the striatum of patients with idiopathic Parkinson's disease. N Engl J Med 1988; 318: 876–80.
Langston JW, Widner H, Goetz CG, Brooks D, Fahn S, Freeman T, et al. Core assessment program for intracerebral transplantations (CAPIT). Mov Disord 1992; 7: 2–13.
Luo C, Song W, Chen Q, Zheng Z, Chen K, Cao B, et al. Reduced functional connectivity in early-stage drug-naive Parkinson's disease: a resting-state fMRI study. Neurobiol Aging 2014; 35: 431–41.
Maier F, Williamson KL, Tahmasian M, Rochhausen L, Ellereit AL, Prigatano GP, et al. Behavioural and neuroimaging correlates of impaired self-awareness of hypo- and hyperkinesia in Parkinson's disease. Cortex 2016; 82: 35–47.
Mattingley JB, Husain M, Rorden C, Kennard C, Driver J. Motor role of human inferior parietal lobe revealed in unilateral neglect patients. Nature 1998; 392: 179–82.
Mohan A, Roberto AJ, Mohan A, Lorenzo A, Jones K, Lapidus KAB, et al. The Significance of the Default Mode Network (DMN) in neurological and neuropsychiatric disorders: a review. Yale J Biol Med 2016; 49–57.
Niethammer M, Eidelberg D. Metabolic brain networks in translational neurology: concepts and applications. Ann Neurol 2012; 72: 635–47.
Obeso JA, Stamelou M, Goetz CG, Poewe W, Lang AE, Weintraub D, et al. Past, present, and future of Parkinson's disease: a special essay on the 200th Anniversary of the Shaking Palsy. Mov Disord 2017; 32: 1264–310.
Ohtsuka C, Sasaki M, Konno K, Koide M, Kato K, Takahashi J, et al. Changes in substantia nigra and locus coeruleus in patients with early-stage Parkinson's disease using neuromelanin-sensitive MR imaging. Neurosci Lett 2013; 541: 93–8.
Pagano G, Niccolini F, Politis M. Imaging in Parkinson's disease. Clin Med 2016; 16: 371–5.
Palop JJ, Chin J, Mucke L. A network dysfunction perspective on neurodegenerative diseases. Nature 2006; 443: 768–73.
Pauli WM, Nili AN, Tyszka JM. A high-resolution probabilistic in vivo atlas of human subcortical brain nuclei. Sci Data 2018; 5: 180063.
Politis M. Neuroimaging in Parkinson disease: from research setting to clinical practice. Nat Rev Neurol 2014; 10: 708–22.
Postuma RB, Dagher A. Basal ganglia functional connectivity based on a meta-analysis of 126 positron emission tomography and functional magnetic resonance imaging publications. Cereb Cortex 2006; 16: 1508–21.
Prodoehl J, Burciu RG, Vaillancourt DE. Resting state functional magnetic resonance imaging in Parkinson's disease. Curr Neurol Neurosci Rep 2014; 14: 448.
Pyatigorskaya N, Gaurav R, Arnaldi D, Leu-Semenescu S, Yahia-Cherif L, Valabregue R, et al. Magnetic resonance imaging biomarkers to assess substantia nigra damage in idiopathic rapid eye movement sleep behavior disorder. Sleep 2017; 40. doi: 10.1093/sleep/zsx149.
R Core Team. R: a language and environment for statistical computing. Vienna, Austria: R Foundation for Statistical Computing; 2018.
Sawle GV, Playford ED, Burn DJ, Cunningham VJ, Brooks DJ. Separating Parkinson's disease from normality. Arch Neurol 1994; 51: 237–43.
Schindlbeck KA, Eidelberg D. Network imaging biomarkers: insights and clinical applications in Parkinson's disease. Lancet Neurol 2018; 17: 629–40.
Schwartz F, Tahmasian M, Maier F, Rochhausen L, Schnorrenberg KL, Samea F, et al. Overlapping and distinct neural metabolic patterns related to impulsivity and hypomania in Parkinson's disease. Brain Imaging Behav 2019; 13: 241–54.
Seeley WW, Crawford RK, Zhou J, Miller BL, Greicius MD. Neurodegenerative diseases target large-scale human brain networks. Neuron 2009; 62: 42–52.
Seibyl J, Russell D, Jennings D, Marek K. Neuroimaging over the course of Parkinson's disease: from early detection of the at-risk patient to improving pharmacotherapy of later-stage disease. Semin Nucl Med 2012; 42: 406–14.
Sharman M, Valabregue R, Perlbarg V, Marrakchi-Kacem L, Vidailhet M, Benali H, et al. Parkinson's disease patients show reduced cortical-subcortical sensorimotor connectivity. Mov Disord 2013; 28: 447–54.
Tahmasian M, Bettray LM, van Eimeren T, Drzezga A, Timmermann L, Eickhoff CR, et al. A systematic review on the applications of resting-state fMRI in Parkinson's disease: does dopamine replacement therapy play a role? Cortex 2015a; 73: 80–105.
Tahmasian M, Eickhoff SB, Giehl K, Schwartz F, Herz DM, Drzezga A, et al. Resting-state functional reorganization in Parkinson's disease: an activation likelihood estimation meta-analysis. Cortex 2017; 92: 119–38.

Tahmasian M, Rochhausen L, Maier F, Williamson KL, Drzezga A, Timmermann L, et al. Impulsivity is associated with increased metabolism in the fronto-insular network in Parkinson's Disease. Front Behav Neurosci 2015b; 9: 317.

Tahmasian M, Shao J, Meng C, Grimmer T, Diehl-Schmid J, Yousefi BH, et al. Based on the network degeneration hypothesis: separating individual patients with different neurodegenerative syndromes in a preliminary hybrid PET/MR Study. J Nucl Med 2016; 57: 410–5.

Teune LK, Bartels AL, Jong BM, de Willemsen ATM, Eshuis SA, de Vries JJ, et al. Typical cerebral metabolic patterns in neurodegenerative brain diseases. Mov Disord 2010; 25: 2395–404.

Tomlinson CL, Stowe R, Patel S, Rick C, Gray R, Clarke CE. Systematic review of levodopa dose equivalency reporting in Parkinson's disease. Mov Disord 2010; 25: 2649–53.

van Eimeren T, Monchi O, Ballanger B, Strafella AP. Dysfunction of the default mode network in Parkinson disease: a functional magnetic resonance imaging study. Arch Neurol 2009; 66: 877–83.

De Virgilio A, Greco A, Fabbrini G, Inghilleri M, Rizzo MI, Gallo A, et al. Parkinson's disease: autoimmunity and neuroinflammation. Autoimmun Rev 2016; 15: 1005–11.

Vo A, Sako W, Fujita K, Peng S, Mattis PJ, Skidmore FM, et al. Parkinson's disease-related network topographies characterized with resting state functional MRI. Hum Brain Mapp 2017; 38: 617–30.

Wang J, Xie S, Guo X, Becker B, Fox PT, Eickhoff SB, et al. Correspondent functional topography of the human left inferior parietal lobule at rest and under task revealed using resting-state fMRI and coactivation based parcellation. Hum Brain Mapp 2017; 38: 1659–75.

Whitfield-Gabrieli S, Nieto-Castanon A. Conn: a functional connectivity toolbox for correlated and anticorrelated brain networks. Brain Connect 2012; 2: 125–41.

Whitfield-Gabrieli S, Nieto-Castanon A. CONN - functional connectivity toolbox v17. 2017. http://www.nitrc.org/projects/conn.

Wu T, Wang J, Wang C, Hallett M, Zang Y, Wu X, et al. Basal ganglia circuits changes in Parkinson's disease patients. Neurosci Lett 2012; 524: 55–9.

Wu T, Wang L, Chen Y, Zhao C, Li K, Chan P. Changes of functional connectivity of the motor network in the resting state in Parkinson's disease. Neurosci Lett 2009; 460: 6–10.

Yau Y, Zeighami Y, Baker TE, Larcher K, Vainik U, Dadar M, et al. Network connectivity determines cortical thinning in early Parkinson's disease progression. Nat Commun 2018; 9: 12.

Zeighami Y, Ulla M, Iturria-Medina Y, Dadar M, Zhang Y, Larcher K-H, et al. Network structure of brain atrophy in de novo Parkinson's disease. eLife 2015; 4.

Zhou J, Gennatas ED, Kramer JH, Miller BL, Seeley WW. Predicting regional neurodegeneration from the healthy brain functional connectome. Neuron 2012; 73: 1216–27.